A direct method for the simultaneous characterization of thermal diffusivities of a bi-layer material consisting of a thin coating deposited on a substrate

Elissa El Rassy, Yann Billaud, Didier Saury

A direct method for the simultaneous characterization of thermal diffusivities of a bi-layer material consisting of a thin coating deposited on a substrate

Elissa EL RASSY[a,b], Yann BILLAUD[a], Didier SAURY[a]

[a]Institut Pprime UPR CNRS 3346 - CNRS ⋄ ENSMA ⋄ Université de Poitiers, 1 avenue Clément Ader, B.P. 40109, F-86961, Futuroscope Chasseneuil CEDEX, FRANCE;
[b]LTEN – UMR CNRS 6607, Université de Nantes, CNRS, Rue Christian Pauc, BP 50609, 44306 Nantes cedex 3, France

Abstract

This work presents a method dedicated to the simultaneous identification of the thermal diffusivities of coatings or thin film materials. To ensure non-destructive thermal characterization of the coating, the present method also implies the identification of the substrate thermal properties, which may be orthotropic. The estimation of thermal diffusivities is based on the resolution of an inverse problem by minimizing the quadratic difference between the response of a 3D semi-analytical model and the measurements resulting from a single '3D flash method' type experiment, using a stochastic based optimization algorithm. A unique non-intrusive test, that consists in recording the temperature change cartography on one face of the sample by means of an infrared camera, is required. The evolution of the temperatures within the material is generated by a non-uniform and almost instantaneous excitation imposed by a CO_2 laser on the measured face. The difficulties related

to the control of the excitation, in terms of the distribution of the imposed flux or the energy absorbed by the material, are overcome by estimating the parameters associated to the excitation simultaneously with the thermal diffusivities. The developed method is applied to estimate the thermal diffusivity of a coating used in thermographic phosphor thermometry to measure wall surface temperatures and heat fluxes in combustion environments. The method is first evaluated on simulated data as a function of the measuring/excitation face in order to ensure the feasibility, the robustness and accuracy of the current method and to establish the best experimental configuration. Experimental results are then exploited and the estimation results are compared with other methods results.
Keywords: Bi-layer material, parameter estimation, flash method, inverse problem, thermal quadrupoles

1. Introduction

Coatings are used in many domains, they can serve as thermal (e.g. insulation) or fire protection), chemical (i.e. erosion, corrosion or oxidation prevention) or mechanical protection (e.g. ablation protection), or to improve optical properties (e.g. black painting to tend toward the emissivity of a black body). It can be also used in the frame of temperature measurement techniques, among those the most common techniques are namely, the "IR thermograhy" and the "phosphorescence thermometry". The latter is based on the phosphorescent properties of phosphoric mixture used to determine the surface temperature from the measurement of the radiation intensity emitted by this surface.

The present work aims to thermally characterize the thin layer, referred hereinafter by "TPT" coating for "Thermographic Phosphor Thermometry", deposed on surfaces of interest in internal combustion engines as the walls of the combustion chamber. The thermal characterization (in particular the thermal diffusivity) of such phosphorous layer is crucial in order to accurately predict the intensity of heat transferred through this coat layer as well as the temperature evolution profile at the surface of the covered material during operating cycles.

However, as it is not desirable to separate the coating from its substrate, the investigated method is based on a direct and simultaneous thermal characterization of samples constituting layers.

In this context, and on the contrary to the thermal characterization of isotropic or orthotropic monolayer materials [1–13] that had paid attention to a large community, very few studies addressed the issues of coatings on substrate materials. Some of these studies have been interested in the characterization of only the thermal conductivity or diffusivity of (i) thin films [14–16] or (ii) coatings on substrates materials [17–25], or (iii) 1D temperature dependent thermal diffusivity (i.e. $a(T)$) of a viscous intumescent coating with a moving boundary system [26]. In those works, a priori knowledge of the substrate properties or a determination of these properties through a previous experiment, is often required [14, 17, 18, 23, 24, 26–30]. Consequently, any error in these properties will be propagated through the model and results in an inaccuracy of the required estimation.

To overcome the difficulty to obtain separately each constituting components, some authors try to identify the thermal diffusivities of the coating

without any knowledge about the substrate properties. This method relies on a two-steps identification technique that allows such measurement but only at very short time [31], limiting this latter one to relatively thick coatings. Any estimation strategy applied for multilayers, or for all layers constituting that multilayers material, and involving more than one step, may propagate error throughout the various stages of estimation. For example, one can cite the method of gobbé et al. [32] in which the in-plane and in-depth thermal conductivities of a multilayers sample are estimated successively by the hot wire and the hot strip methods, or a strategy developed by Li et al. [33] in order to characterize both layers (i.e. the coating and the substrate), by repeating the experiment/measurements several times. Very few studies have been focused on simultaneous estimation of each isotropic layer thermal diffusivities, in a multilayer or a coating on substrate bi-layered structure. One can cite some works that have attempted to simultaneously estimate, in cylindrical coordinates, the two-dimensional diffusivities of the anisotropic coatings deposited on an isotropic substrate, but with very limited results [27, 28].

The present study concerns the simultaneous estimation, i.e. using a unique step, via a non-intrusive flash experiment, of the thermal diffusivity of the coating and its substrate. The current case of a coating or a thin layer deposited on a substrate is a particular case of bilayer materials in which the thickness of the deposit is very small compared to the substrate. The identification proposed in the framework of this study is based on a direct estimation method that minimizes the quadratic difference between the measurements resulting from a single 'flash' type experiment inspired

from [34] carried out by an IR camera, and the outputs of a direct pseudo-analytical model based on the "3D thermal quadrupoles" method [35].

Considering the relative complexity and non-linearity of the direct model, and in order to converge towards the global optimum (minimum) instead of a local one, the desired parameters are identified by applying a hybrid optimization algorithm. The latter combines a global minimisation performed by a particle-type swarm optimization algorithm (PSO) [36] followed by a local minimisation carried out by a gradient based method.

First, the direct model and the estimation method are presented. The estimation is then carried out on a bilayer material composed of a thin phosphorus layer deposited on a low diffusivity substrate. The feasibility and the robustness of the overall method is demonstrated based on simulated noisy data. The results obtained by considering two experimental configurations and different assumptions concerning the thermal nature of the substrate (isotropic or orthotropic), are then presented and discussed.

2. Problem description

2.1. ***General principle***

The main aim of this part concerns the thermal characterization of a specific two-layers material constituted of a thin layer or coating deposited on an isotropic or orthotropic material. The coating considered in this study is the a phosphorescent material generally applied in the combustion chambers for temperature measurements. In order to reproduce, as well as possible, the experimental deposition of the TPT coating, the coating should be deposited on a metallic sample, such as copper or aluminum. However, these materials

are highly diffusive and due to some experimental limitations related to the achievable acquisition frequency of the handled IR camera, these substrates necessitating a very high acquisition frequency (typically $> 1000\ Hz$) are replaced by a substrate having a low thermal diffusion (e.g. HDPE = High Density Polyethylene or polyamide) that requires a moderate acquisition frequency ($\simeq 50$ Hz). The identification of thermophysical properties of such complex materials is generally based on the resolution of an inverse heat conduction problem (IHCP).

2.2. ***Inverse Heat Conduction Problem (IHCP)***

This section presents the general principle of inverse problems and each element involved in the overall procedure. It contains general briefing of each element of the general procedure and its current application in the present method.

[Figure 1 about here.]

The IHCP general principle consists in comparing the "observables" Y^* obtained from experimental or synthetic measurements with those resulting from an analytical or numerical model ($Y(\beta)$) that must, as much as possible, mimic the experiment. Thereby, the model has to provide outputs $Y(\beta)$ that must i) be compatible with the measurements Y^* and ii) be dependent on the parameters to estimate β. This last point is discussed further in the section dedicated to the sensitivity analysis. This comparison is performed by means of a cost function f, also called "objective function". As long as this function f does not satisfy a certain criterion, the optimization algorithm adjusts the input parameters β of the direct model. The process is repeated until the

procedure converges to the optimal set of parameters $\hat{\beta}$ with the admissible values, i.e the one that minimizes the difference between the experiment and the model.

For an experimental application, the major sections investigated in the identification technique will be mainly:

- The experiment
- The direct model
- The comparison of observable quantities via a cost function
- The minimization via an identification algorithm

The overall estimation strategy concept is illustrated in Fig. 1 that presents the connection between the elements involved in the inverse problem resolution. The various steps of the estimation strategy are detailed and discussed in the following sections. The estimation method developed in this work is referred as DSEH (Direct and Simultaneous Estimation using Harmonics).

2.2.1. ***Experimental 3D flash method***

The experiment protocol corresponds to an unconventional and 3D flash technique qualified as a non-intrusive method, both in terms of excitation and measurements. In this method, the sample that should be thermally characterized is subjected to a localized and non-uniform thermal excitation using a CO_2 laser. The resulting surface temperature evolution cartography is continuously measured, during the cooling phase. These measurements are performed by an IR camera, at the front or rear faces of the material.

Figs. 2 represent the experimental setup and the equipment used to generate the experimental data.

[Figure 2 about here.]

The specifications of the main devices are detailed hereafter:

- The infrared camera, that is a FLIR SC7000 having n adjustable frequency (up to 200 Hz), and a resolution of 320×256 pixels (full frame).
- The laser is a CO_2 laser (DIAMOND GEM-Series by Coherent©), having an adjustable power and duration time.

2.2.2. ***Direct bi-layered model***

The identification method proposed in this study is based on a three-dimensional analytical heat transfer model that mimics the flash technique. This model describes the transient heat conduction within a homogeneous and opaque bilayer material, being exposed to a non-uniform and almost instantaneous thermal excitation.

As shown in Fig. 3, the two layers have the same dimensions in the XY plane ($l_{x_1} = l_{x_2} = l_x$ and $l_{y_1} = l_{y_2} = l_y$). The lateral faces are assumed to be thermally isolated, while the front and rear faces are subjected to convective and radiation losses described by a linearized global heat exchange coefficient that is assumed to be equal to a constant and uniform term on both sides, $h_f = h_b = h$, with $h = 10\ W \cdot m^{-2} \cdot K^{-1}$, a commonly accepted value for this kind of experimental exercise.

In addition, at time $t = 0$, the system is supposed to be in thermal equilibrium at T_∞. It is important to underline that all the temperatures

considered in this model are relative to the temperature of the environment (i.e. $T(x, t = 0) = 0$). The thermal resistance at the interface between the two layers is neglected. In addition, the thermal excitation must be chosen in such a way to generate a sufficient temperature elevation to be accurately measured, but at the same time moderate enough to be able to consider the thermophysical properties as constant and independent on temperature variation. The system of partial differential equations that describes the heat transfers within the bi-layered system, the conditions at the interfaces, and the boundary and initial conditions are presented herebelow.

[Figure 3 about here.]

The set of differential partial equations modeling the associated heat transfers inside the medium (layer 1 and 2) as well as the condition at interface, and the initial and boundaries conditions (IC & BC) are presented hereafter. In these equations, T refers to the temperature relative to the ambiant temperature (T_∞):

$$\begin{aligned} \text{layer 1}: \quad & \frac{\partial T_1}{\partial t} = a_{x_1}\frac{d^2T_1}{dx^2} + a_{y_1}\frac{d^2T_1}{dy^2} + a_{z_1}\frac{d^2T_1}{dz^2} \quad \text{for } z \in [0, l_{z_1}],\ t > 0 \\ \text{layer 2}: \quad & \frac{\partial T_2}{\partial t} = a_{x_2}\frac{d^2T_2}{dx^2} + a_{y_2}\frac{d^2T_2}{dy^2} + a_{z_2}\frac{d^2T_2}{dz^2} \quad \text{for } z \in [l_{z_1}, l_{z_1} + l_{z_2}],\ t > 0 \end{aligned} \tag{1}$$

$$\begin{aligned} \text{Interface:} \quad & \lambda_{z_1}\frac{\partial T_1(z = l_{z_{1-}})}{\partial z} = \lambda_{z2}\frac{\partial T_2(z = l_{z_{1+}})}{\partial z} \quad \text{for } z = l_{z_1}\ ,\ t > 0 \\ & T_2(z = l_{z_{1+}}) = T_1(z = l_{z_{1-}}) \qquad \text{for } z = l_{z_1}\ ,\ t > 0 \end{aligned} \tag{2}$$

$$\begin{aligned}
\text{BC1:} \quad -\lambda_{x_1}\frac{\partial T_1}{\partial x} &= 0 && \text{for } x=0 \text{ and } x=l_x,\ t>0 \qquad (3)\\
-\lambda_{y_1}\frac{\partial T_1}{\partial y} &= 0 && \text{for } y=0 \text{ and } y=l_y,\ t>0\\
-\lambda_{z_1}\frac{\partial T_1}{\partial z} &= -h_f\cdot T_1+\phi^{ex}_{x,y}(t) && \text{for } z=0,\ t>0\\
\text{BC2:} \quad -\lambda_{x_2}\frac{\partial T_2}{\partial x} &= 0 && \text{for } x=0 \text{ and } x=l_x,\ t>0 \qquad (4)\\
-\lambda_{y_2}\frac{\partial T_2}{\partial y} &= 0 && \text{for } y=0 \text{ and } y=l_y,\ t>0\\
-\lambda_{z_2}\frac{\partial T_2}{\partial z} &= -h_b\cdot T_2 && \text{for } z=l_{z_1}+l_{z_2},\ t>0
\end{aligned}$$

$$\text{IC:} \quad T_1(x,y,z)=0,\ T_2(x,y,z)=0 \quad \text{for } t=0 \qquad (5)$$

In the considered case, the thermal resistance at the interface between both layers is neglected. After getting the harmonics $\xi_{m,n}(z,p)$ by projection of the physical relative temperature $T(x,y,z,t)$ into space Fourier cosine and Laplace domain, the three dimensional analytical solution can be obtained using the thermal quadrupoles formalism as follows:

$$\begin{pmatrix} \xi_{m,n}(z=0,p) \\ \phi^{ex}_{m,n}(p)-h_f\xi_{m,n}(z=0,p) \end{pmatrix} = \begin{pmatrix} A_{m,n}(p) & B_{m,n}(p) \\ C_{m,n}(p) & D_{m,n}(p) \end{pmatrix} \times \begin{pmatrix} \xi_{m,n}(z=l_{z_1}+l_{z_2},p) \\ h_b\cdot\xi_{m,n}(z=l_{z_1}+l_{z_2},p) \end{pmatrix} \qquad (6)$$

with:

$$\xi_{m,n}(z,p)=\frac{1}{l_x\cdot l_y}\int_{t=0}^{\infty}\int_{y=0}^{l_y}\int_{x=0}^{l_x} T(x,y,z,t)\cdot\cos\left(\frac{m\pi x}{L_x}\right)\cdot\cos\left(\frac{n\pi y}{L_y}\right)\cdot e^{-pt}\,dx\,dy\,dt \qquad (7)$$

$$\phi^{ex}_{m,n}(p) = \frac{1}{l_x \cdot l_y} \int_{t=0}^{\infty} \int_{y=0}^{l_y} \int_{x=0}^{l_x} \phi^{ex}_{x,y}(t) \cdot \cos\left(\frac{m\pi x}{L_x}\right) \cdot \cos\left(\frac{n\pi y}{L_y}\right) \cdot e^{-pt}\, dx\, dy\, dt \tag{8}$$

and

$$\begin{pmatrix} A_{m,n}(p) & B_{m,n}(p) \\ C_{m,n}(p) & D_{m,n}(p) \end{pmatrix} = \begin{pmatrix} a_{m,n,1} & b_{m,n,1} \\ c_{m,n,1} & d_{m,n,1} \end{pmatrix} \times \begin{pmatrix} a_{m,n,2} & b_{m,n,2} \\ c_{m,n,2} & d_{m,n,2} \end{pmatrix} \tag{9}$$

where:

$$a_{m,n,i\in\{1,2\}} = \cosh(l_{z_i} \cdot K_{m,n,i}(p)) \tag{10}$$

$$b_{m,n,i\in\{1,2\}} = \frac{\sinh(l_{z_i} \cdot K_{m,n,i}(p))}{\lambda_{z_i} \cdot K_{m,n,i}(p)} \tag{11}$$

$$c_{m,n,i\in\{1,2\}} = \lambda_{z_i} \cdot K_{m,n,i}(p) \cdot \sinh(l_{z_i} \cdot K_{m,n,i}(p))) \tag{12}$$

$$d_{m,n,i\in\{1,2\}} = a_{m,n,i}(p) \tag{13}$$

$$K_{m,n,i}(p) = \sqrt{\frac{p}{a_{z_i}} + \alpha_m^2 \frac{a_{x_i}}{a_{z_i}} + \beta_n^2 \frac{a_{y_i}}{a_{z_i}}}; \quad \alpha_m = \tfrac{m\pi}{l_x}; \quad \beta_n = \frac{n\pi}{l_y}$$

The resulting analytical expressions of the rear ($l_z = l_{z_1} + l_{z_2}$) and front ($l_z = 0$) face normalized harmonics are respectively:

$$\xi_{m,n}(z = l_{z_1} + l_{z_2}, p) = \frac{\phi^{ex}_{m,n}(p)}{C_{m,n}(p) + D_{m,n}(p) \cdot h_b + A_{m,n}(p) \cdot h_f + B_{m,n}(p) \cdot h_f \cdot h_b} \tag{14}$$

$$\begin{aligned} \xi_{m,n}(z = 0, p) &= \xi_{m,n}(z = l_{z_1} + l_{z_2}, p) \cdot [A_{m,n}(p) + B_{m,n}(p) \cdot h_b] \\ &= \frac{\phi^{ex}_{m,n}(p) \cdot (A_{m,n}(p) + B_{m,n}(p) \cdot h_b)}{C_{m,n}(p) + D_{m,n}(p) \cdot h_b + A_{m,n}(p) \cdot h_f + B_{m,n}(p) \cdot h_f \cdot h_b} \end{aligned} \tag{15}$$

These normalized harmonics are then projected into the real time domain using De-Hoog inversion technique, and $\xi^{mod}_{m,n}(\beta, z = 0 \text{ or } z = l_{z_1} + l_{z_2}, t)$ will

represent the model outputs involved in the inverse problem technique and estimation strategy.

Note that, the process under which the coating layer is deposited on the surface of the substrate encourage the consideration of a negligible contact resistance Rc at the interface between both layers. In Addition, assuming the excitation source can be modeled as $\phi^{ex}_{x,y}(t) = \phi_0 \cdot F_{x,y}(x,y) \cdot u(t)$ leads to $\phi^{ex}_{m,n}(p) = \frac{\phi_0 \cdot F_{m,n} \cdot u(p)}{l_x \cdot l_y} = R_{m,n} \cdot u(p)$, $R_{m,n}$ being the normalized Fourier cosine projection of the excitation shape and $u(p)$ the Laplace transform of the excitation time evolution.

2.2.3. ***Cost function***

The cost function, also known as objective function, is the quadratic deviation between the measured signal and the signal predicted by the direct physical model. Thus, the estimator used for the minimization of the cost function for the front face, is written as follows:

$$\hat{\beta} = \arg\min[f(\beta)] = \min_{\beta} \sqrt{\sum_{m=0}^{M}\sum_{n=0}^{N}[\xi^{mod}_{m,n}(\beta, z=0,t) - \xi^{exp}_{m,n}(t)]^2} \qquad (16)$$

In this method, the considered harmonics are equally weighted. The first term of Eq.16, i.e. $\xi^{mod}_{m,n}(\beta,t)$, corresponds to the temporal normalized harmonics at the front face, achieved by the Laplace inversion (De Hoog Algorithm) which is applied to the direct model outputs (Eq.15). The second term, $\xi^{exp}_{m,n}(t)$, represents the observables issued from front face relative temperature measurement, projected in Fourier Cosine space:

$$\xi^{exp}_{m,n}(t) = \frac{1}{l_x \cdot l_y}\int_{y=0}^{l_y}\int_{x=0}^{l_x} T^{exp}(x,y,z,t)\cdot\cos\left(\frac{m\pi x}{L_x}\right)\cdot\cos\left(\frac{n\pi y}{L_y}\right) dx\, dy \quad (17)$$

Given that the harmonics of low spatial frequencies hold the largest quantity of information related to diffusivities, the exploited harmonics in this study will be the first even modes: $(m, n) = \{0, 2, 4, 6\} \times \{0, 2, 4, 6\}$. The odd harmonics are thus not considered in the estimation. In fact, here they can be considered as negligible (when compared to even ones), since the excitation spot is centered and exhibits revolution symmetries. Centering can be improved by IR images post treatments, whereas the revolution symmetry is strongly connected to the excitation source. The framing of the images should be performed in a way that guarantees these last assumptions.

The TPT coating is considered isotropic, i.e. $a_{x_{\text{coat}}} = a_{y_{\text{coat}}} = a_{z_{\text{coat}}} = a_{TPT}$, thus the parameters vector β that should be estimated is $\beta = [a_{x,1}, a_{y,1}, a_{z,1}, a_{TPT}, R_{0,0}, R_{0,2}, R_{2,2} \dots R_{m,n} \dots R_{6,6}]$ for the case where the substrate is considered as orthotropic. In that case, 20 parameters must be estimated. However, for the case where the substrate is also considered as isotropic, the vector parameter becomes $\beta = [a_{HDPE}, a_{TPT}, R_{0,0}, R_{0,2}, R_{2,2} \dots R_{m,n} \dots R_{6,6}]$ and then 18 parameters have to be identified simultaneously.

2.2.4. ***Optimization algorithm***

Hybrid optimization algorithm is applied in the current study to minimize the cost function (Eq.16) and find the optimal parameter vector $\hat{\beta}$. The relatively complex estimation problem and the non-linear nature of the phenomenon require the use of a stochastic approach in order to seek the global minimum and avoid getting stuck into a local minimum. Thanks to a coupled stochastic-deterministic optimization algorithm, a global search of the minimum region is achieved by using a Particle Swarm Optimization (PSO) algorithm [36–38], followed by a local search of the cost function minimum

value, which carried out by the gradient based method (interior point method [39]). All algorithm implementations details are well described in [2].

3. Numerical Applications

3.1. ***Sensitivity analysis***

A study of reduced sensitivities is conducted here in order to determine the most appropriate configurations for the estimation of the coating properties, with or without the simultaneous estimation of the substrate properties. Reduced sensitivities are defined as:

$$Sr_{m,n}(\beta_j, t) = \frac{\partial Y(\beta, t)}{\partial \beta_j} \times \beta_j \Big|_{\beta_{k \neq j}} \tag{18}$$

The reduced sensitivities (Eq.18) have then similar units (and so similar scale values). Thus, they can properly ensure a comparison of the different parameters impacts on the model outputs [40, 41].

[Figure 4 about here.]

The classification of the 4 different cases that are investigated to find the most suitable experimental configuration, is shown in Fig. 4a. The sensitivity of the harmonic $\xi_{2,2}(t)$ to the coating in-depth thermal diffusivity, and for the four possible configurations, is presented in Fig. 4b. It is important to note that the sensitivity analysis that allows to compare different possible experimental configurations, and the numerical applications represented in 3 require the values of the parameters β or at least approximative values, in order to obtain synthetic data via the direct model (Eq.15. These values are

inspired from the literature [42] and from a study [43] that considered the case of a high-speed thermographic phosphor thermometry used to control the temperature increase and the time and position of flame impingement at the piston surface. These values are gathered in table 1.

[Table 1 about here.]

An exploitation window with $l_x = l_y = 50\ mm$ has been proved, through a preliminary study [44], to be suitable for such application, since it can give a good accuracy/time ratio. The parameters involved in the thermal excitation definition correspond to the total amount of energy deposited on the material, $Q = 0.56\ J$, and to the laser radius r $= \frac{l_x}{9.55} (\approx 5\ mm)$ (coherent with previous experimental observations).

While remaining consistent in terms of radius value that can be experimentally generated, this set of parameters can guarantee a temperature evolution at the surface of the material: i) sufficient to be accurately measured and ii) tolerable to avoid any risk of thermophysical properties modification (i.e. temperature dependence of parameters) that can occur at high temperature (typically $> 10\ °C$).

In these numerical applications, the spatial distribution of the thermal excitation has been parameterized by a cubic polynomial shape, which is consistent with experimental observations and already tested in previous monolayers applications [2]. This form allows us to calculate the form factors $F_{m,n}$ in the Fourier cosine space.

The normalized shape of the excitation is described, along the x-axis,

$$F_x(x) = \frac{1}{r} \times \begin{cases} 1 - 3 \cdot (\frac{x}{r})^2 - 2(\frac{x}{r})^3 & \text{for } -r \leq x < 0 \\ 1 - 3 \cdot (\frac{x}{r})^2 + 2(\frac{x}{r})^3 & \text{for } 0 \leq x < r \\ 0 & \text{otherwise} \end{cases} \quad (19)$$

The cosine Fourier transform in the x-direction of the previous function $F_x(x)$ is

$$\begin{aligned} F_m &= \int_0^{l_x} F_x(x - \frac{l_x}{2}) \times cos(\frac{m \cdot \pi \cdot x}{l_x}) dx \\ F_m &= \frac{-24\Big(cos(\frac{m \cdot \pi}{2}) \cdot \big(cos(\alpha_m \cdot r) - 1 + \frac{\alpha_m \cdot r}{2} \cdot sin(\alpha_m \cdot r)\big)\Big)}{r^4 \cdot \alpha_m^4} \end{aligned} \quad (20)$$

The same function is used in the y-direction with $F_y(y)$. Consequently, the shape function associated with the laser beam, $F_{x,y}(x, y) = F_x(x) \cdot F_y(y)$, in the cosine-Fourier domain, leads to the following $F_{m,n}$ shape factor:

$$F_{m,n} = \frac{24^2}{r^8 \cdot \alpha_m^4 \cdot \beta_n^4} \cdot \Bigg[\Big(cos(\frac{m \cdot \pi}{2}) \cdot \big(cos(\alpha_m \cdot r) - 1 + \frac{\alpha_m \cdot r}{2} \cdot sin(\alpha_m \cdot r)\big)\Big) \cdot \Big(cos(\frac{n \cdot \pi}{2}) \cdot \big(cos(\beta_n \cdot r) - 1 + \frac{\beta_n \cdot r}{2} \cdot sin(\beta_n \cdot r)\big)\Big)\Bigg] \quad (21)$$

In that case, the normalized shape factor in the Fourier-cosine space $R_{m,n}$ is such as $R_{m,n} = \frac{\phi_0 \cdot F_{m,n}}{l_x \cdot l_y}$.

3.2. ***Numerical and Experimental configurations***

Two possible experimental configurations are considered for numerical validation in order to test the feasibility and the accuracy of the identification method for both cases. The FF-FF (see Fig. 4a) configuration is the most

sensitive, as shown in Fig. 4b. The other configuration BF-BF (see Fig. 4a) corresponds to the simplest one, in terms of experimental conditions and limitations. Their respective experimental protocols are illustrated in Fig. 5. The FF-FF configuration (case (a) in Fig. 5) consists in deposing the source heat flux $\phi^{ex}_{x,y}(t)$ on the surface of the coating and measuring the resulting temperature evolution profile at the same side. On the contrary, the BF-BF configuration (case (b) in Fig. 5) considers the case where the excitation and the temperature profiles measurements are carried out at the substrate surface side.

[Figure 5 about here.]

The excitation of the thin coating surface side (occuring in the configurations FF-FF and FF-BF) is not advisable, due to the degradation and poor control of heat penetration depth reasons. The same observations can be made for the temperature measurements at this surface (configurations FF-FF and BF-FF) due to the ill-knowledge of the TPT surface emissivity.

3.3. ***Parameters initialization***

In addition to the general parameters described in [36], the PSO algorithm specifications and conditions as well as the stopping criteria, are tabulated in the Table 2. The stopping criterion is a combination of several conditions. The iterative minimization will be stopped (i) if the maximum number of iterations is achieved, or (ii) if the number of stall iterations without any significant change and with a best value of the cost function less than the tolerance value, exceeds the maximum stall iterations. Furthermore, following the PSO principle, the swarms particles move in the domain field,

predefined by a upper and a lower bounds, seeking for the optimal solution i.e. for the lowest value of the cost function (Eq.16). One can find also the bounds of the parameters values that should be estimated in Table 2.

[Table 2 about here.]

3.4. ***Numerical results and discussion***

The numerical exercise currently conducted in order to validate the identification feasibility and evaluate the robustness and the accuracy of the estimation method, relies on "synthetic measurements" for both configurations FF-FF (case (a)) and BF-BF (case (b)). These data are generated from the direct model for which a random noise with a Gaussian distribution is added, in order to mimic experimental conditions.

The overall procedure is shown in Fig. 6. This technique is used to evaluate the feasibility of an estimation method, compare different methods or adjust the estimation method parameters. The same model being used twice, it is clear that the success in retrieving the parameter does not ensure the success when applying the method to experimental data. The method does not detect any errors in the model or mismatch between the model and the experiment. However, this strategy may be considered as a preliminary validation of the overall estimation strategy.

[Figure 6 about here.]

Once the model is validated, this strategy is used to check the feasibility of the estimation procedure, in terms of parameters correlations, and adequacy of optimization algorithm. In addition, it is used to perform parametric

studies in order to define the optimal algorithm parameters for each case under consideration.

The numerical results for both experimental configurations (a) and (b) and for both cases with isotropic or orthotropic substrate, and with or without random noise added (up to 5%), are presented in Table 3 for a 2 mm HDPE substrate covered by a 50 μm TPT coating. These calculations are repeated for 3 mm HDPE substrate covered by a 300 μm TPT coating (see Table 3) in order to be coherent with experimental applications, that follows this section.

[Table 3 about here.]

Results in table 3 are presented in terms of relative deviation or error between the parameters values used to generate the synthetic data and those estimated using the current identification investigated in thin study. They prove the feasibility of the identification method developed for such bi-layered materials.

3.5. ***Optimal configuration selection***

It can obviously be noticed in table 3 the small relative deviation between the original values and the estimated ones for all treated cases, with and without random Gaussian noise added. The comparison validate therefore the robustness and accuracy of the current method. Not surprisingly, the configuration (a)-FF-FF, gives theoretically better results compared to the configuration (b)-BF-BF and notably without adding noise to the original signal generated by the direct model (with a relative error $< 2.1 \cdot 10^{-3}$ % without noise and < 1.9 % with 5 % noise for the 2 mm HDPE covered by

50 μm of TPT, and a relative error $< 1.0 \cdot 10^{-3}$ % without noise and < 1.9 % with 5 % noise for the 3 mm HDPE covered by 300 μm of TPT). Despite this, results obtained with the configuration (b)-BF-BF are also convincing and promising, specially when adding a certain level of noise (with a relative error $< 6.2 \cdot 10^{-2}$ % without noise and < 1.4 % with 5 % noise for the 2 mm HDPE covered by 50 μm of TPT, and a relative error $< 1.0 \cdot 10^{-2}$ % without noise and < 2 % with 5 % noise for the 3 mm HDPE covered by 300 μm of TPT).

[Figure 7 about here.]

In fact, this latter configuration (BF-BF) is more suitable from the experimental points of view, as it limits the risk of coating degradation that can take place within the configuration (a)-FF-FF. Adding to that, impulse model is difficult to realize for the configuration (a)-FF-FF, due to the ill-knowledge of the coating thermal characteristic time and the necessity of a high acquisition frequency to detect the dynamic of heat transfer through this thin layer. Nevertheless, the total acquisition time required for the configuration (a)-FF-FF is quite lower than that required with the configuration (b)-BF-BF. This intuitive observation is confronted by sensitivity study for the observables to the diffusivities of both layers. The reduced sensitivities for the mode $(m = 2, n = 2)$, generally considered as the reference one [45], are plotted in Figs. 7 for both configurations and for the case where both layers are considered as isotropic.

This study proved that the identification of thermal diffusivities is possible at short time for the case (a)-FF-FF, whereas the case (b)-BF-BF requires

a longer duration time, due to the substrate properties and its thickness. Lastly, accounting all restrictions and risks that could be faced within the configuration (a)-FF-FF and the good accuracy level that could be achieved within the configuration (b)-BF-BF, this latter will be preferred for experimental applications presented thereafter.

4. Experimental applications

Experimental applications have been carried out on samples constituted of a HDPE layer of 3 mm thichness covered by a thermal phosphorescent coating whose thicknesses are between 300 and 350 μm. These samples were provided and manufactured by the "Institut Français du Pétrole et Energies Nouvelles" (IFPEN). A photography of one of these samples is shown in Fig. 8a.

[Figure 8 about here.]

As already argued and demonstrated in 3.5, the configuration (b)-BF-BF that consists of an excitation and temperature evolution measurement, both conducted at the material rear face (substrate side), is used. In this case, the substrate layer should be painted by a black thin layer of known emissivity, as shown in Fig. 8b, in order to control the surface emissivity and to have relatively high surface absorption of the laser beam that generates the heat excitation.

The identification technique was conducted first on these samples, using the values of the density ρ and heat capacity C that are found in the literature (Table 4). In addition, the density ρ and heat capacity C were measured using

399 a calorimeter, a digital balance and a digital micrometer. The measured
400 values and the level of uncertainties are also indicated in Table 4. These
401 measures were also used for the identification and compared in the next
402 section to the results obtained with the data found in the literature. Note
403 that, all PSO algorithm specifications and stopping criteria, as well as the
404 particles seeking bounds, are the same as those used in the numerical exercise
405 and tabulated in the Table 2.

406 [Table 4 about here.]

407 Adding to these physical properties, the dimension of the exploitation
408 window, namely the size of the frames, $l_x \times l_y$, have to respect the compromise
409 between a sufficient size in order to respect the boundary conditions and
410 restricted size to avoid the degradation of the data (by dilution of the signal
411 in the background signal). Thus, the exploitation window is chosen such as
412 $l_x \times l_y = 35,8\ mm \times 37.5\ mm$ for the sample 1 and $l_x \times l_y = 22,8\ mm \times 24.7\ mm$
413 for the sample 2, while conserving a symmetric excitation and a centered spot,
414 as mentioned in section 2.2.3.

415 *4.1.* ***Experimental results and discussion***

416 The results corresponding to the sample 1 (3 mm HDPE ; 300 μm of TPT
417 coating) and sample 2 (3 mm HDPE ; 350 μm TPT coating) are tabulated
418 in Table 5. The variance-covariance matrix of the estimated parameters (see
419 Eq. A.7 in Appendix A for further details) is calculated and the standard
420 deviations of the results are presented into brackets in Tables 5, 6 and 7.

421 [Table 5 about here.]

Regarding the substrate layer, relatively thick compared to the coating layer and typically quasi-isotropic, its thermal diffusivities have been identified using a "2D" reference method known as ENH [10, 31] (Estimation using Normalization of Harmonics). Results are also reported in Table 6 for in-plane diffusivities. Values obtained with the current DSEH method (Tab. 5) for these same in-plane diffusivities are also reported in this table.

[Table 6 about here.]

The thermal conductivity of the TPT coating in both samples can be deduced with $\lambda_{TPT} = \rho \cdot C \cdot a_{TPT} = 0.525\ W \cdot m^{-1} \cdot K^{-1}$ for sample 1 and $0.540\ W \cdot m^{-1} \cdot K^{-1}$ for sample 2.

These estimations are repeated using the density ρ and heat capacity C values that are measured (Table 4) on sample 1. The results obtained for this sample are summarized in Table 7.

[Table 7 about here.]

First of all, Table 5 shows that the thermal diffusivities identified for both samples are close to each other, which can be considered as a promising results. From Table 5 it can be also observed that the isotropic character (i.e. $a_x \approx a_y \approx a_z$) of HDPE is verified for both samples. For sample 1, $diag(\bar{\bar{a}}_{HDPE}) = [0.274, 0.259, 0.278]\ mm^2 \cdot s^{-1}$ and for sample 2, $diag(\bar{\bar{a}}_{HDPE}) = [0.265, 0.265, 0.279]\ mm^2 \cdot s^{-1}$. Furthermore, these values are coherent with those found in the literature [42] ($a_{HDPE-[42]} \in [0.260 - 0.288]\ mm^2 \cdot s^{-1}$), and are in a very good agreement with results obtained using ENH method (see Table 6) for the substrate.

Regarding the TPT coating, estimated diffusivities values are found, using measured thermal properties, $\lambda_{TPT} = 0.500 \pm 0.077\ W \cdot m^{-1} \cdot K^{-1}$ for sample 1 and $\lambda_{TPT} = 0.510 \pm 0.078\ W \cdot m^{-1} \cdot K^{-1}$ for sample 2, to be in good agreement with that retrieved by Benoit Fond team from Magdeburg: $\lambda_{TPT} = 0.47 \pm 0.07\ W \cdot m^{-1} \cdot K^{-1}$ who conducted a contact thermal characterization method, the "hot disk" method [46]. Adding to that, the estimated values are in the same order of magnitude than those presented in [43]. It should be notice that the composition (i.e. solvent used) and the mixing ratio may vary according to the manufacturing process, and explain the slight discrepancy observed here.

Finally a small difference in the results can be observed when repeating the estimation procedure with the measured values of $\rho \cdot C$, as shown in Table 7. It is also demonstrated that the influence of errors propagation from the a priori known properties on the estimation results, appears to be neglected.

4.2. ***Results accuracy evaluation: consistency between experimental and numerical results***

Finally, in order to illustrate the consistency of the method, evolution of the first experimental harmonics $\xi_{m,n}^{exp}(z = 0, t)$ are compared with the estimated harmonics $\xi_{m,n}^{est}(\hat{\beta}, z = 0, t)$ in Fig. 9, for the sample 1. The discrepancy between experimental and estimated data are represented by residual lines that illustrate the great fit between the experimental and the estimated signals. It should be noticed that the highest deviation is always observed in the normalized harmonic $\xi_{0,0}$ (mean field) which is often highly affected by the environmental changes.

[Figure 9 about here.]

5. Conclusion

The proposed identification method is applied on a specific degenerated case of two-layer material constituted of a thin coating deposited on an isotropic or orthotropic substrate. First, a numerical exercise considering a TPT coating involved in phosphorescence thermometry and deposited on an HDPE layer, is carried out using noisy synthetic data within two possible experimental configurations. For some technical limitations, this coating was deposited on a HDPE polymer substrate layer. This kind of deposit is usually encountered in the engines internal combustion chambers for wall temperature measurements. Among the two experimental configurations tested, one consists in exciting and measuring the temperature evolution at the coating side while the other configuration considers the case where excitation and measurements are conducted at the substrate surface side. Based on convincing estimation results, sensitivity analysis, and experimental limitations, the last configuration (excitation and measurement on the substrate side) has been proved more convenient for such exercise. Then, the identification has been experimentally carried out on two different samples and gave very promising results. In addition, the values of the polymer diffusivites verifying the isotropic character of this latter, and are in good agreements with the literature values as well as with the ENH in-plane estimation method. Regarding the coating, estimated values are in the same order of magnitudes with those found in the literature, and in good agreements with other research team results obtained using a contact characterization method. Each element of the method, which allows the simultaneous estimation of the thermal diffusivity tensors of each constituting layers, is described and discussed.

Among these elements, the pseudo-analytic model and the hypothesis on which it is based, as well as the estimation method used to minimize the discrepancy between the outputs of the model and the measurement, are presented. The materials of the sample have been chosen in such a way to be able to neglect the thermal contact resistance between layers. The samples have been carefully prepared to reach a perfect contact between both layers. In general, thermal contact resistance is significant and may dominate for relatively highly heat conductors such as metals, or for relatively thin layer (having thicknesses in the order of nanometers, which is not the case here where TPT coatings have thicknesses between 50 to 300 micrometers). It can be neglected for the association of relatively low heat conductors such as the TPT coating deposited on polymers such as the HDPE substrate.

Acknowledments

The Authors thank the European Union and the Nouvelle Aquitaine District for their financial support through the CPER/FEDER 2014-2020 programs. The Authors also thank IFPEN that manufactures and provides test samples.

Appendix A. Variance-Covariance Matrix

The Variance-Covariance Matrix is frequently used as a testing tool for characterizing the solutions dispersion, and is considered as one of the most important estimator properties. Typically, this matrix quantifies the estimations dispersion among the expected value. The best and the most accurate

estimator is the one having the lowest variance, in such a way the estimations $\hat{\beta}$ slightly vary when switching the input data. The deepest is the information extraction from observables Y^*, the lowest are the standard deviations/variances of the estimations β. The estimation variance-covariance matrix is noticed $cov(\hat{\beta})$, of dimension $n_\beta \times n_\beta$, and is consistent with the ordinary least square (OLS).

When assuming that the measurement noise is non-correlated with a standard deviation of σ_{noise}, and that variances are similar for all observations Y^* (homoscedasticity hypothesis), therefore one can apply the following correlation, given in [47]:

$$cov(\hat{\beta}) = \sigma^2_{noise}[S^T S]^{-1} \tag{A.1}$$

Where S is the sensitivity matrix defined in the following equations:

$$S_{m,n}(\beta_j, t) = \left.\frac{\partial Y(\beta, t)}{\partial \beta_j}\right|_{\beta_{k\neq j}} = \left.\frac{\partial \xi_{m,n}(\beta, t)}{\partial \beta_j}\right|_{\beta_{k\neq j}} \tag{A.2}$$

In this study the measurement noise is assumed Gaussian, additive and constant in time, and it can be qualified by i.i.d (independent and identically distributed). Based on the calculations developed by Ruffio in [45], when working with normalized harmonics $\xi_{m,n}$, the diagonal coefficients of the variance-covariance matrix are the variances $\sigma^2_{m,n}$ of harmonics and are given by:

$$\sigma^2_{m,n} = \frac{\sigma^2_m}{4 \cdot (N_x \times N_y)}(1 + \delta_m) \cdot (1 + \delta_n) \tag{A.3}$$

$$\delta_m = \begin{cases} 1 & \text{if } m = 0, \\ 0 & \text{otherwise} \end{cases} \quad \text{and} \quad \delta_n = \begin{cases} 1 & \text{if } n = 0, \\ 0 & \text{otherwise} \end{cases} \tag{A.4}$$

534 $\sigma_{m,n}$ refers here to the standard deviation corresponding to each harmonic
535 and are obtained by an IR camera having $N_x \times N_y$ pixels (depending on the
536 exploitation window size at each treated case). The standard deviation of
537 each pixel is $\sigma_m = 0.1\ ^\circ C$. Therefore, Eq.A.3 entails:

$$\frac{\sigma_m^2}{4 \cdot (N_x \times N_y)} \leq \sigma_{m,n}^2 \leq \frac{\sigma_m^2}{(N_x \times N_y)} \tag{A.5}$$

538 All harmonics are assumed to have the same standard deviations (the worst
539 case scenario), equal to that corresponding to the mean field, i.e. m=n=0.
540 Consequently,

$$\sigma_{m,n}^2 = \sigma_{0,0}^2 = \frac{\sigma_m^2}{(N_x \times N_y)} = \frac{0.1^2}{(N_x \times N_y)} \tag{A.6}$$

541 which finally leads to:

$$cov(\hat{\beta}) = \sigma_{m,n}^2 [S^T S]^{-1} = \frac{0.1^2}{(N_x \times N_y)} [S^T S]^{-1} \tag{A.7}$$

Nomenclature

Latin Symbols

$\overline{\overline{a}}$	Thermal diffusivity tensor	$m^2 \cdot s^{-1}$
a_x, a_y, a_z	Thermal diffusivities	$m^2 \cdot s^{-1}$
C	Thermal Capacity	$J \cdot kg^{-1} \cdot K^{-1}$
f	Cost function	(-)
$F_{x,y}$	Shape function associated with the laser beam	(-)
$F_{m,n}$	Fourier coefficients of the shape function	(-)
h	Overall heat transfer coefficient	$W \cdot m^{-2} \cdot K^{-1}$
l_x, l_y, l_z	Sample's dimensions	m
M, N	Harmonics maximum indices	(-)
p	Laplace variable	(-)
$R_{m,n}$	Excitation factor	$W \cdot m^{-2}$
Rc	Thermal contact resistance	$K \cdot m^2 \cdot W^{-1}$
r	Laser spot radius	m
S	Sensitivity	K
Sr	Reduced Sensitivity	K
T	Temperature elevation	K
T_∞	Environment temperature	K
$u(t)$	Time shape function of the laser beam	(-)
$X_m(x)$	Basis function in the x-plane	(-)
$Y_n(y)$	Basis function in the y-plane	(-)
Y^*	Observables	K
$Y(\beta)$	Model outputs	K

Greek symbols

α_m, β_n	Harmonic pulsations	$rad \cdot m^{-1}$
β	Parameter vector to be estimated	(-)
$\hat{\beta}$	Optimal parameters vector	(-)
ρ	Density	$kg \cdot m^{-3}$
$\lambda_x, \lambda_y, \lambda_z$	Thermal conductivities	$W \cdot m^{-1} \cdot K^{-1}$
σ	Standard deviation	(-)
$\xi_{m,n}(t)$	Normalized harmonics in time domain	K
$\xi_{m,n}(p)$	Normalized harmonics in Laplace domain	$K \cdot s$
ϕ_0	Amount of energy absorbed by the sample	J
$\phi^{ex}_{m,n}(p)$	Excitation in the Fourier and Laplace domains	$W \cdot m^{-2} \cdot s$
$\phi^{ex}_{x,y}(t)$	Excitation in the physical and time domains	$W \cdot m^{-2}$

Subscripts and Superscripts

ex	Excitation
exp	Experiment
f,b	Front and back faces
m,n	Spatial Fourier modes
T	Transpose symbol
x,y	Cartesian coordinates

Abbreviations

BF	Back face
Config	Configuration

DSEH	Direct and Simultaneous Estimation using Harmonics
ENH	Estimation using Normalization of Harmonics
ERH	Estimation using Ratio of Harmonics
FF	Front face
HDPE	High Density Polyethylene
OLS	Ordinary Least Square Estimator
PSO	Particle swarm optimization
Rel.	Relative
TPT	Thermographic Phosphor Thermometry

References

[1] C. Rodiet, B. Remy, A. Degiovanni, Thermal characterization of anisotropic materials by integral transforms taking into account the thermal coupling with the sample-holder, International Journal of Thermal Sciences 79 (Supplement C) (2014) 67–75.

[2] E. El Rassy, Y. Billaud, D. Saury, Simultaneous and direct identification of thermophysical properties for orthotropic materials, Measurement 135 (2019) 199 – 212.

[3] Y. Souhar, B. Rémy, A. Degiovanni, Thermal Characterization of Anisotropic Materials at High Temperature Through Integral Methods and Localized Pulsed Technique, International Journal of Thermophysics 34 (2) (2013) 322–340.

[4] E. Ruffio, D. Saury, D. Petit, Robust experiment design for the estimation of thermophysical parameters using stochastic algorithms, International Journal of Heat and Mass Transfer 55 (11) (2012) 2901 – 2915. doi:https://doi.org/10.1016/j.ijheatmasstransfer.2012.02.008.
URL http://www.sciencedirect.com/science/article/pii/S0017931012000713

[5] E. El Rassy, Y. Billaud, D. Saury, Flash method experiment design for the thermal characterization of orthotropic materials, Measurement Science and Technology.

[6] W. P. Adamczyk, R. A. Białecki, T. Kruczek, Retrieving thermal con-

ductivities of isotropic and orthotropic materials, Applied Mathematical Modelling 40 (4) (2016) 3410–3421.

[7] S. Graham, D. L. McDowell, R. B. Dinwiddie, Multidimensional Flash Diffusivity Measurements of Orthotropic Materials, International Journal of Thermophysics 20 (2) (1999) 691–707.

[8] M. Thomas, N. Boyard, N. Lefèvre, Y. Jarny, D. Delaunay, An experimental device for the simultaneous estimation of the thermal conductivity 3-D tensor and the specific heat of orthotropic composite materials, International Journal of Heat and Mass Transfer 53 (23) (2010) 5487–5498.

[9] V. Plana, Caractérisation par méthode inverse et modélisation des propriétés thermophysiques orthotropes des matériaux composites, Theses, Toulouse, ENSAE (Jan. 2003).
URL http://www.theses.fr/2003ESAE0004

[10] J.-C. Krapez, L. Spagnolo, M. Frieß, H.-P. Maier, G. Neuer, Measurement of in-plane diffusivity in non-homogeneous slabs by applying flash thermography, International Journal of Thermal Sciences 43 (10) (2004) 967–977.

[11] W. P. Adamczyk, S. Pawlak, Z. Ostrowski, Determination of thermal conductivity of cfrp composite materials using unconventional laser flash technique, Measurement 124 (2018) 147–155.

[12] G. Wróbel, Z. Rdzawski, G. Muzia, S. Pawlak, Determination of thermal diffusivity of carbon/epoxy composites with different fiber content

using transient thermography, Journal of achievements in materials and manufacturing engineering 37 (2) (2009) 518–525.

[13] G. Wróbel, S. Pawlak, G. Muzia, Thermal diffusivity measurements of selected fiber reinforced polymer composites using heat pulse method, Archives of Materials Science and Engineering.

[14] M. Akabori, Y. Nagasaka, A. Nagashima, Measurement of the thermal diffusivity of thin films on substrate by the photoacoustic method, International Journal of Thermophysics 13 (3) (1992) 499–514.

[15] S. W. Kim, R. E. Taylor, Estimation of thermophysical properties of a film coated on a substrate using pulsed transient analysis, International Journal of Thermophysics 14 (1) (1993) 135–147.

[16] S. Orain, Y. Scudeller, S. Garcia, T. Brousse, Use of genetic algorithms for the simultaneous estimation of thin films thermal conductivity and contact resistances, International Journal of Heat and Mass Transfer 44 (20) (2001) 3973 – 3984.

[17] F. Rigollet, F. Papini, D. Boisson, Identification optimale des propriétés thermophysiques d'un revêtement, Comptes Rendus de l'Académie des Sciences - Series IV - Physics 1 (1) (2000) 111–117.

[18] I. Perry, B. Remy, D. Maillet, Thermal Characterization of a Multilayer Material Through the Flash Method, Journal of Thermophysics and Heat Transfer 20 (2) (2006) 231–237.

[19] O. Faugeroux, B. Claudet, S. Bénet, J. J. Serra, D. Boisson, Caractérisation thermophysique de revêtements par méthode photother-

mique impulsionnelle en face avant, International Journal of Thermal Sciences 43 (4) (2004) 383–401.

[20] L. Chen, A. M. Limarga, D. R. Clarke, A new data reduction method for pulse diffusivity measurements on coated samples, Computational Materials Science 50 (1) (2010) 77–82.

[21] M. Akoshima, T. Baba, M. Ogawa, T. Tanaka, Y. Harada, A. Kawasaki, F. Ono, Thermal Diffusivity Measurements of the Layered Materials by the Laser Flash Method, Materials Science Forum 631-632 (2010) 103–108.

[22] M. Akoshima, T. Tanaka, S. Endo, T. Baba, Y. Harada, Y. Kojima, A. Kawasaki, F. Ono, Thermal Diffusivity Measurement for Thermal Spray Coating Attached to Substrate Using Laser Flash Method, Japanese Journal of Applied Physics 50 (11S).

[23] B. Hay, J.-R. Filtz, J. Hameury, G. Davée, L. Rongione, O. Enouf, Thermal-Diffusivity Measurement of Ceramic Coatings at High Temperature using "Front-Face" and "Rear-Face" Laser Flash Methods, International Journal of Thermophysics 30 (4) (2009) 1270–1282.

[24] G. H. He, J. D. Guo, Y. Y. Zhang, B. Q. Wang, B. L. Zhou, Measurement of Thermal Diffusivity of Thermal Control Coatings by the Flash Method Using Two-Layer Composite Sample, International Journal of Thermophysics 21 (2) (2000) 535–542.

[25] J.-L. Battaglia, A. Kusiak, M. Bamford, J.-C. Batsale, Photothermal radiometric characterization of a thin deposit using a linear swept-

frequency heat flux waveform, International Journal of Thermal Sciences 45 (11) (2006) 1035 – 1044.

[26] L. Perez, L. Autrique, M. Gillet, Implementation of a conjugate gradient algorithm for thermal diffusivity identification in a moving boundaries system, in: Journal of Physics: Conference Series, Vol. 135(1), IOP Publishing, 2008, p. 012082.

[27] N. D. Milošević, M. Raynaud, K. D. Maglić, Simultaneous Estimation of the Thermal Diffusivity and Thermal Contact Resistance of Thin Solid Films and Coatings Using the Two-Dimensional Flash Method, International Journal of Thermophysics 24 (3) (2003) 799–819.

[28] N. Milošević, Mesure de la diffusivité thermique et de la résistance de contact thermique des couches minces sur des substrats par la méthode impulsionnelle, Lyon, INSA, 2008.

[29] J.-L. Battaglia, A. Kusiak, M. Bamford, J.-C. Batsale, Photothermal radiometric characterization of a thin deposit using a linear swept-frequency heat flux waveform, International Journal of Thermal Sciences 45 (2006) 1035 – 1044.

[30] W. P. Adamczyk, T. Kruczek, G. Moskal, R. A. Białecki, Nondestructive technique of measuring heat conductivity of thermal barrier coatings, International Journal of Heat and Mass Transfer 111 (Supplement C) (2017) 442–450.

[31] P. Bison, F. Cernuschi, E. Grinzato, In-depth and In-plane Thermal Diffusivity Measurements of Thermal Barrier Coatings by IR Camera:

667 Evaluation of Ageing, International Journal of Thermophysics 29 (6)
668 (2008) 2149–2161.

669 [32] C. Gobbé, S. Iserna, B. Ladevie, Hot strip method: application to ther-
670 mal characterisation of orthotropic media, International Journal of Ther-
671 mal Sciences 43 (10) (2004) 951–958.

672 [33] B. Li, L. Pottier, J. P. Roger, D. Fournier, E. Welsch, Thermal character-
673 ization of film-on-substrate systems with modulated thermoreflectance
674 microscopy, Review of Scientific Instruments 71 (5) (2000) 2154–2160.

675 [34] W. J. Parker, R. J. Jenkins, C. P. Butler, G. L. Abbott, Flash Method
676 of Determining Thermal Diffusivity, Heat Capacity, and Thermal Con-
677 ductivity, Journal of Applied Physics 32 (9) (1961) 1679–1684.

678 [35] D. Maillet, S. André, J. C. Batsale, A. Degiovanni, C. Moyne, Thermal
679 quadrupoles: solving the heat equation through integral transforms, Wi-
680 ley, 2000.

681 [36] J. Kennedy, Swarm Intelligence, in: Handbook of Nature-Inspired and
682 Innovative Computing, Springer, Boston, MA, 2006, pp. 187–219.

683 [37] Q. Bai, Analysis of Particle Swarm Optimization Algorithm, Computer
684 and Information Science 3 (1) (2010) 180.

685 [38] I. C. Trelea, The particle swarm optimization algorithm: convergence
686 analysis and parameter selection, Information Processing Letters 85 (6)
687 (2003) 317–325.

[39] R. Waltz, J.L. Morales, J. Nocedal, D. Orban, An interior algorithm for nonlinear optimization that combines line search and trust region steps (2006).

[40] D. Petit, D. Maillet, Techniques inverses et estimation de paramètres. Partie 1 (Jan. 2008).

[41] D. Petit, D. Maillet, Techniques inverses et estimation de paramètres. Partie 2 (Jan. 2008).

[42] Polyethylene - High density - online catalog source - supplier of research materials in small quantities - Goodfellow.
URL `http://www.goodfellow.com/A/Polyethylene-High-density.html`

[43] C.-P. Ding, R. Honza, B. Böhm, A. Dreizler, Simultaneous measurement of flame impingement and piston surface temperatures in an optically accessible spark ignition engine, Applied Physics B 123 (4) (2017) 110.

[44] E. El Rassy, Y. Billaud, D. Saury, Unconventional flash technique for the identification of multilayer thermal diffusivity tensors, International Journal of Thermal Sciences (2020) in press.

[45] E. Ruffio, D. Saury, D. Petit, Improvement and comparison of some estimators dedicated to thermal diffusivity estimation of orthotropic materials with the 3d-flash method, International Journal of Heat and Mass Transfer 64 (2013) 1064–1081.

[46] M. Gustavsson, E. Karawacki, S. E. Gustafsson, Thermal conductivity, thermal diffusivity, and specific heat of thin samples from transient

measurements with hot disk sensors, Review of Scientific Instruments 65 (12) (1994) 3856–3859.

[47] E. Ruffio, Estimation de paramètres et de conditions limites thermiques en conduction instationnaire pour des matériaux anisotropes, Chasseneuil-du-Poitou, Ecole nationale supérieure de mécanique et d'aérotechnique, 2011.
URL http://www.theses.fr/2011ESMA0019

List of Figures

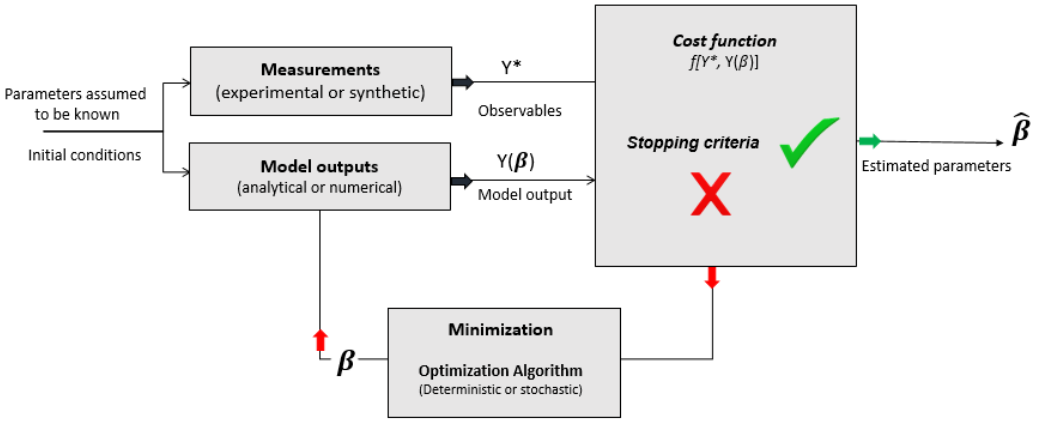

Figure 1: Inverse problem principle and main sections (steps).

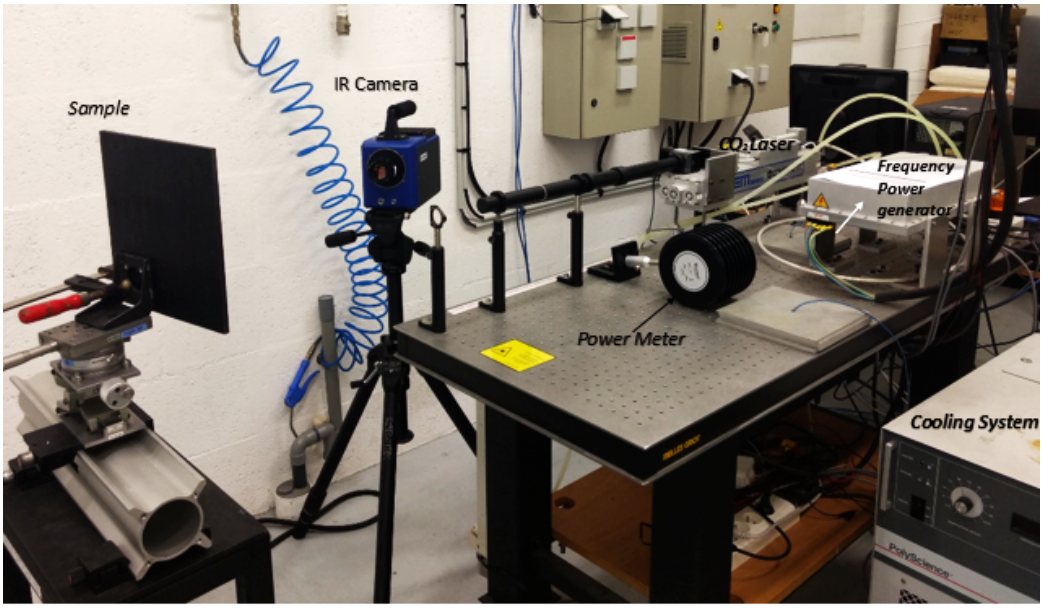

Figure 2: Experimental setup representing the front face flash method and including the main devices involved in the measurement procedure : the sample, CO_2 laser and IR camera.

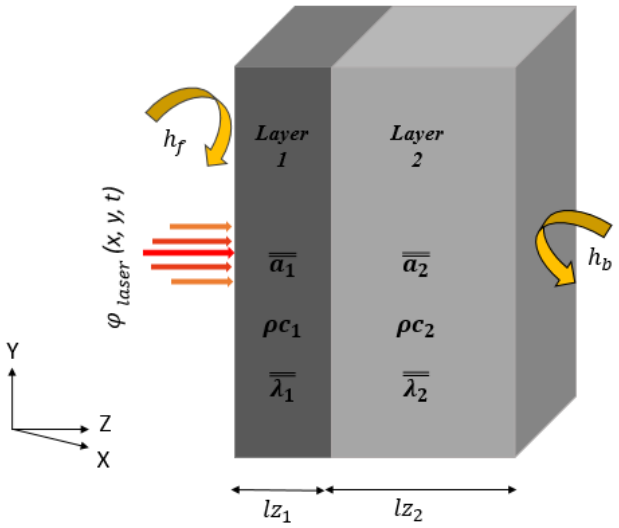

Figure 3: Homogeneous two-layer plane material subjected to non-uniform flash excitation at the front face.

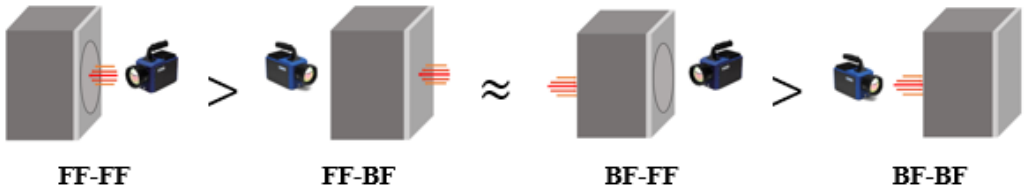

(a)

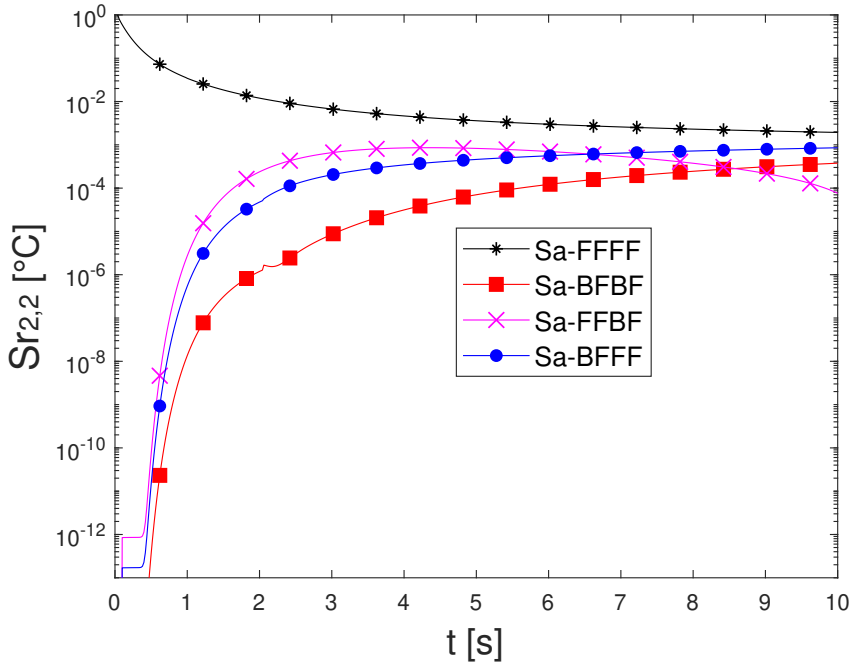

(b)

Figure 4: Sensitivity evolution of the harmonic $\xi_{2,2}(t)$ to the coating in depth thermal diffusivity, for the four possible configurations.

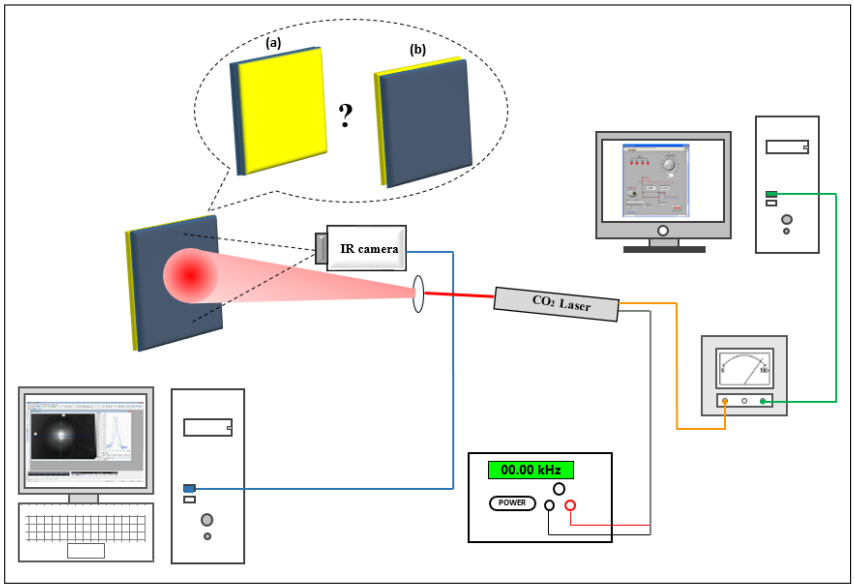

Figure 5: The numerically tested and compared experimental configurations, dedicated to the thermal characterization of the TPT coating.

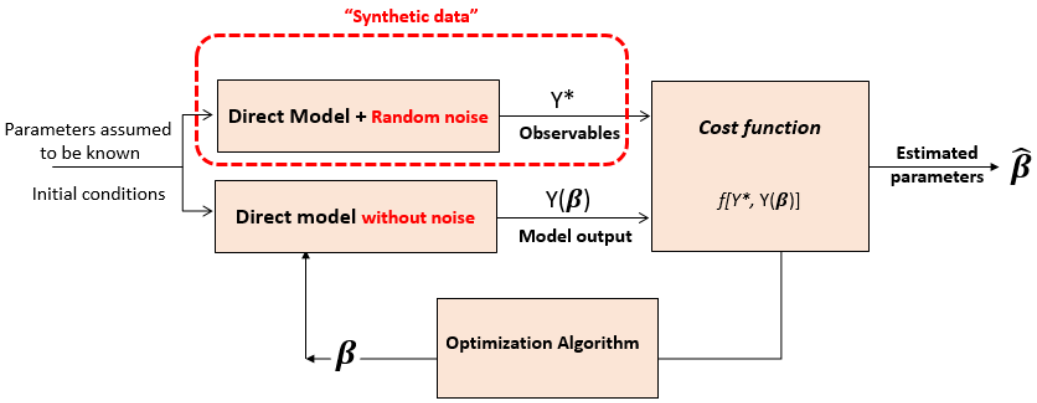

Figure 6: Numerical application principle

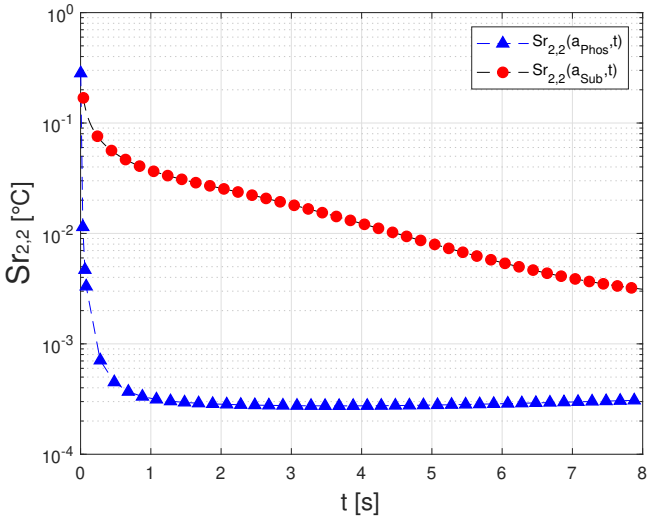

(a) Configuration(a)

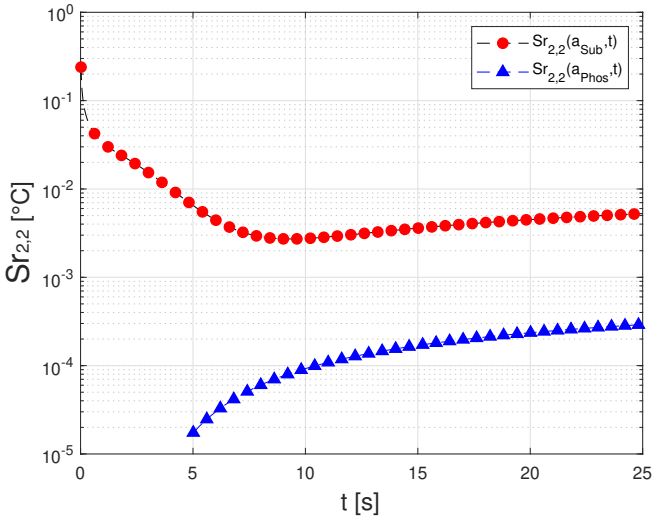

(b) Configuration(b)

Figure 7: The evolution of normalized harmonics $\xi_{2,2}$ reduced sensitivities to the in-depth thermal diffusivities of both layers, and for both configurations (a) and (b).

(a) TPT coating over a HDPE substrate - Coating side

(b) Black painted HDPE - Substrate side

Figure 8: Experimental application on the two-layers material constituted by a TPT-coating deposited over HDPE substrate

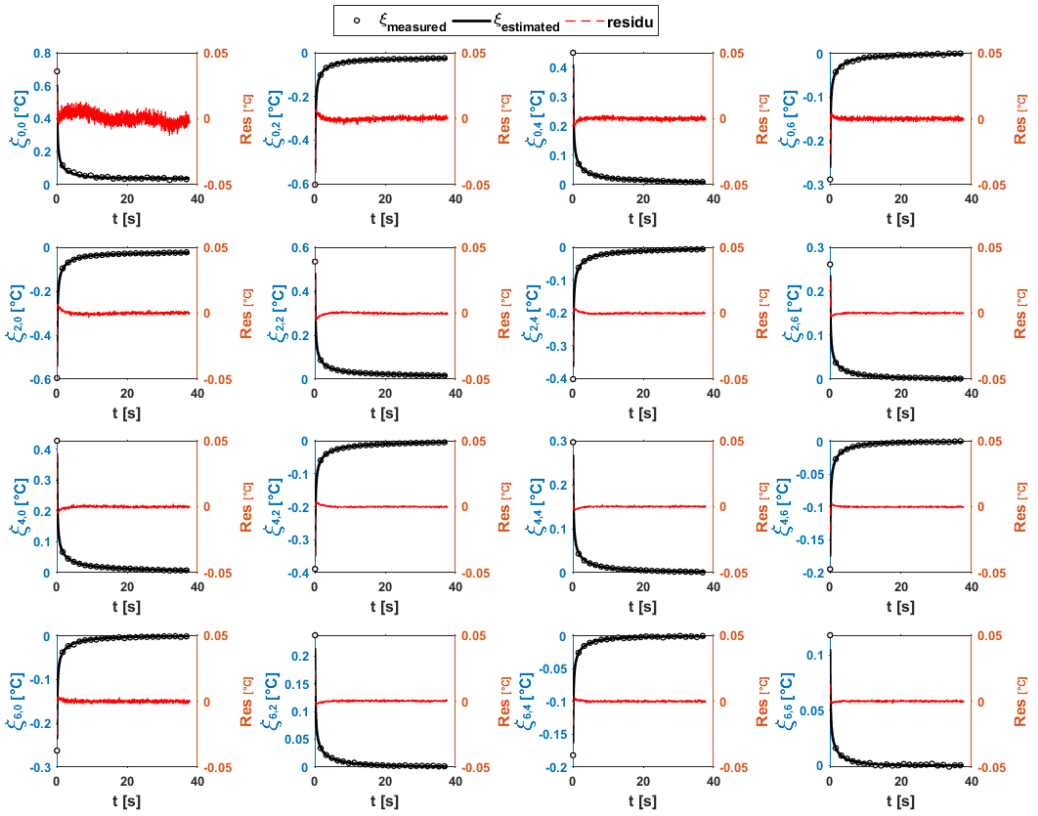

Figure 9: Front face normalized harmonics evolution related to experimental data and reconstructed data by means of estimated parameters, in addition to the residu, for the sample 1.

List of Tables

Parameters	**TPT coating** [43]	**HDPE** [42]
$a\ [mm^2 \cdot s^{-1}]$	[0.30 - 1.00]	2.77
$\rho C\ [kJ \cdot m^{-3} \cdot K^{-1}]$	1316	1805
$l_z\ [mm]$	[0.05 - 0.30]	[2.0 - 3.0]

Table 1: Model parameters values used to generate synthetic measures signals.

Conditions	**Values**
Bounds of $\overline{\overline{a_1}}$ and $\overline{\overline{a_2}}$	$[10^{-9}; 10^{-4}]\ m^2 \cdot s^{-1}$
Bounds of $R_{m,n}$	$[-100; +100]\ W \cdot m^2$
Number of PSO particles	50
Maximum iterations	$500\times$ size of β
Maximum stop (stall) iterations	20
Tolerance value	10^{-8}
Maximum time	$+\infty$
Maximum stall time	$+\infty$
Minimum objective value	$-\infty$

Table 2: PSO specifications, and stopping criteria selected for the estimation procedure.

Configuration			Config.(a) / FF-FF		Config.(b) / BF-BF	
Case ($e_{TPT} = 50\ \mu m$ / $e_{HDPe} = 2\ mm$)		noise level / Rel. deviation %	0%	5%	0%	5%
1	isotropic substrate	$\frac{\lvert\Delta a\rvert}{a}$	$5.37 \cdot 10^{-4}$%	0.50%	$1.39 \cdot 10^{-3}$%	0.51%
	isotropic coating	$\frac{\lvert\Delta a\rvert}{a}$	$2.06 \cdot 10^{-3}$%	1.81%	$6.18 \cdot 10^{-2}$%	1.33%
2	orthotropic substrate	$\frac{\lvert\Delta a_x\rvert}{a_x}$	$2.56 \cdot 10^{-4}$%	1.40%	$1.69 \cdot 10^{-3}$%	1.02%
		$\frac{\lvert\Delta a_y\rvert}{a_y}$	$2.84 \cdot 10^{-4}$%	0.66%	$1.64 \cdot 10^{-3}$%	0.45%
		$\frac{\lvert\Delta a_z\rvert}{a_z}$	$1.77 \cdot 10^{-4}$%	0.16%	$2.83 \cdot 10^{-4}$%	0.33%
	isotropic coating	$\frac{\lvert\Delta a\rvert}{a}$	$5.61 \cdot 10^{-4}$%	0.45%	$2.74 \cdot 10^{-2}$%	0.42%
Case ($e_{TPT} = 300\ \mu m$ / $e_{HDPe} = 3\ mm$)		noise level / Rel. deviation %	0%	5%	0%	5%
1	isotropic substrate	$\frac{\lvert\Delta a\rvert}{a}$	$1.22 \cdot 10^{-4}$%	1.88%	$8.16 \cdot 10^{-4}$%	0.84%
	isotropic coating	$\frac{\lvert\Delta a\rvert}{a}$	$3.01 \cdot 10^{-4}$%	1.24%	$2.83 \cdot 10^{-3}$%	1.22%
2	orthotropic substrate	$\frac{\lvert\Delta a_x\rvert}{a_x}$	$3.71 \cdot 10^{-4}$%	0.68%	$6.13 \cdot 10^{-4}$%	0.95%
		$\frac{\lvert\Delta a_y\rvert}{a_y}$	$3.15 \cdot 10^{-4}$%	0.69%	$6.19 \cdot 10^{-4}$%	0.85%
		$\frac{\lvert\Delta a_z\rvert}{a_z}$	$6.96 \cdot 10^{-4}$%	1.21%	$1.51 \cdot 10^{-3}$%	0.85%
	isotropic coating	$\frac{\lvert\Delta a\rvert}{a}$	$9.20 \cdot 10^{-4}$%	1.86%	$9.01 \cdot 10^{-3}$%	1.88%

Table 3: Estimation results in function of the presupposed nature of the substrate (isotropic or orthotropic) for a 2 mm HDPE covered by a 50 μm TPT coating and a 3 mm HDPE covered by a 300 μm of TPT coating with $a_{HDPE} = 2.77\ mm^2 \cdot s^{-1}$ and $a_{TPT} = 1\ mm^2 \cdot s^{-1}$.

Parameters	**Values from literature** [43][42]	**Measured values**
$\rho_{HDPE}\ [kg \cdot m^{-3}]$	950	897 ± 16
$C_{HDPE}\ [J \cdot kg^{-1} \cdot K^{-1}]$	1900	1950 ± 58
$\rho_{TPT}\ [kg \cdot m^{-3}]$	2800	3131 ± 110
$C_{TPT}\ [J \cdot kg^{-1} \cdot K^{-1}]$	470	400 ± 12

Table 4: Values required for the experimental identification.

Estimated parameters	**Sample 1**	**Sample 2**
$a_{xHDPE}\ [mm^2 \cdot s^{-1}]$	$0.274\ (\sigma = 1.41 \cdot 10^{-3}, 0.52\%)$	$0.265\ (\sigma = 9.50 \cdot 10^{-4}, 0.36\%)$
$a_{yHDPE}\ [mm^2 \cdot s^{-1}]$	$0.259\ (\sigma = 1.41 \cdot 10^{-3}, 0.55\%)$	$0.265\ (\sigma = 9.50 \cdot 10^{-4}, 0.36\%)$
$a_{zHDPE}\ [mm^2 \cdot s^{-1}]$	$0.278\ (\sigma = 1.9 \cdot 10^{-4}, 0.069\%)$	$0.279\ (\sigma = 1.4 \cdot 10^{-4}, 0.049\%)$
$a_{TPT}\ [mm^2 \cdot s^{-1}]$	$0.399\ (\sigma = 0.035, 8.85\%)$	$0.411\ (\sigma = 0.025, 6.20\%)$

Table 5: Experimental results for sample 1 constituted of a 3 mm HDPE covered by a 300 μm TPT coating and sample 2 constituted of a 3 mm HDPE covered by a 350 μm TPT coating.

Estimated parameter ($mm^2.s^{-1}$)	**Sample 1**		**Sample 2**	
	DSEH	ENH	DSEH	ENH
$a_{x\,HDPE}$	0.274	0.277 $\sigma = 6.73 \cdot 10^{-3}(2.43\%)$	0.265	0.263 $\sigma = 3.92 \cdot 10^{-3}(1.49\%)$
$a_{y\,HDPE}$	0.259	0.257 $\sigma = 9.78 \cdot 10^{-3}(3.80\%)$	0.265	0.267 $\sigma = 6.34 \cdot 10^{-3}(2.37\%)$

Table 6: Comparison of thermal diffusivities of HDPE using DSEH and ENH methods.

Estimated parameters	**Using literature values**	**Using measured values**
$a_{xHDPE}\ [mm^2 \cdot s^{-1}]$	$0.274\ (\sigma = 1.41 \cdot 10^{-3}, 0.52\%)$	$0.273\ (\sigma = 1.41 \cdot 10^{-3}, 0.52\%)$
$a_{yHDPE}\ [mm^2 \cdot s^{-1}]$	$0.259\ (\sigma = 1.41 \cdot 10^{-3}, 0.55\%)$	$0.259\ (\sigma = 1.41 \cdot 10^{-3}, 0.55\%)$
$a_{zHDPE}\ [mm^2 \cdot s^{-1}]$	$0.278\ (\sigma = 1.9 \cdot 10^{-4}, 0.069\%)$	$0.278\ (\sigma = 1.9 \cdot 10^{-4}, 0.069\%)$
$a_{TPT}\ [mm^2 \cdot s^{-1}]$	$0.399\ (\sigma = 0.035, 8.85\%)$	$0.407\ (\sigma = 0.035, 8.69\%)$

Table 7: Experimental identification results using the measured values, compared to previous results using literature values of some parameters.